

# Two-color continuous-variable quantum entanglement in a singly resonant optical parametric oscillator

Domenico Cuzzo\* and Gian-Luca Oppo

*ICS, SUPA, and Department of Physics, University of Strathclyde, Glasgow G4 0NG, Scotland, United Kingdom*

(Received 8 June 2011; published 5 October 2011)

We apply the input-output theory of optical cavities to formulate a quantum treatment of a continuous-wave singly resonant optical parametric oscillator. This case is mainly relevant to highly nondegenerate signal and idler modes. We show that both intensity and quadrature squeezing are present and that the maximum noise reduction below the standard quantum limit is the same at the signal and idler frequencies as in the doubly resonant case. As the threshold of oscillation is approached, however, the intensity-difference and quadrature spectra display a progressive line narrowing which is absent in the balanced doubly resonant case. By use of the separability criterion for continuous variables, the signal-idler state is found to be entangled over wide ranges of the parameters. We show that attainable levels of squeezing and entanglement make singly resonant configurations ideal candidates for two-color quantum information processes, because of their ease of tuning in experimental realizations.

DOI: [10.1103/PhysRevA.84.043810](https://doi.org/10.1103/PhysRevA.84.043810)

PACS number(s): 42.50.Lc, 42.50.Dv, 42.65.Yj

## I. INTRODUCTION

Squeezed states of light, where the noise in one quadrature of the fields is reduced below the vacuum level, are important elements in several applications, such as sub-shot-noise phase measurements [1,2], interferometric detection of gravitational radiation [3,4], and quantum information with continuous variables [5]. In the last case, squeezed states are used to generate continuous-variable entanglement and achieve high fidelity in quantum teleportation protocols [5]. To squeeze quantum fluctuations of the electromagnetic field one needs nonlinear optical effects such as parametric down-conversion or four-wave mixing [6]. In parametric down-conversion a pump photon at frequency  $\omega_p$  splits into a photon at frequency  $\omega_s$ , the signal, and another at  $\omega_i$ , the idler, by interacting with a nonlinear crystal with a second-order nonlinear susceptibility  $\chi^{(2)}$  [6]. The strong nonlinearities required to achieve large noise reductions are, however, uncommon in many crystals. To overcome this limitation, optical cavities are used to form an optical parametric oscillator (OPO). In this case, by setting the device into resonance at the desired frequencies, the oscillation buildup inside the cavity increases noise reduction by considerably extending the interaction time. Theoretical and experimental efforts in nondegenerate cases have mainly concerned the doubly (or even triply) resonant configurations where both the signal and idler fields are resonant [7–9]. The singly resonant cavity is in principle a simpler configuration to realize experimentally but, to the best of our knowledge, theoretical investigations of squeezing and entanglement of the light from a singly resonant OPO (SROPO) are missing. One of the reasons is that SROPOs operate with strongly nondegenerate frequencies while much of the literature on squeezing focuses on the degenerate or close-to-degeneracy cases [10,11]. Recent interest in nonclassical correlations of the strongly nondegenerate regime of parametric down-conversion [12] makes the study of entanglement in SROPOs

important for the optimization of coherent sources with fluctuations below the shot-noise level. There are clear technical advantages for SROPO configurations: only resonance of the signal field has to be maintained, and continuous temperature tuning and suppression of mode hopping are possible. It is the aim of this work to investigate the squeezing and entanglement properties of a SROPO when signal and idler fields have large frequency separations (two-color case). Our approach is similar to what has been used in the case of second-harmonic generation [13,14], namely, a two-photon loss model in which a cavity mode is coupled quadratically to a continuum of output modes rather than linearly, as usual in the input-output formulation of optical cavities.

## II. QUANTUM LANGEVIN EQUATION

We consider parametric down-conversion in a monolithic cavity, resonant with the signal field only, and pumped with a monochromatic classical beam of amplitude  $\alpha_p$  at frequency  $\omega_p$  (see Fig. 1). By assuming perfect collinear phase matching and considering energy conservation, one has [6]

$$\vec{k}_p = \vec{k}_s + \vec{k}_i, \quad (1)$$

$$\omega_p = \omega_s + \omega_i, \quad (2)$$

where  $\vec{k}_p$ ,  $\vec{k}_s$ , and  $\vec{k}_i$  are the wave vectors of the pump, the signal, and the idler fields, respectively. In the case of perfect phase matching, the frequencies of the signal and idler fields depend only on the frequency of the pump and the orientation of the crystal with respect to the direction of the pump beam. The quantum-mechanical Hamiltonian for the system in the rotating-wave approximation is

$$H = H_{\text{sys}} + H_{\text{bath},1} + H_{\text{bath},2} + H_{\text{int},1} + H_{\text{int},2} + H_{\text{int},3}, \quad (3)$$

where  $H_{\text{sys}}$  is the sum of the free energies for the single signal mode  $a_s$  and the continuum of idler modes  $b(\omega)$  treated here within the approach of [15];  $H_{\text{bath},1}$  is the free energy of bosonic heat bath modes  $c_1(\omega)$  providing a description

\*domenico.cuzzo@strath.ac.uk

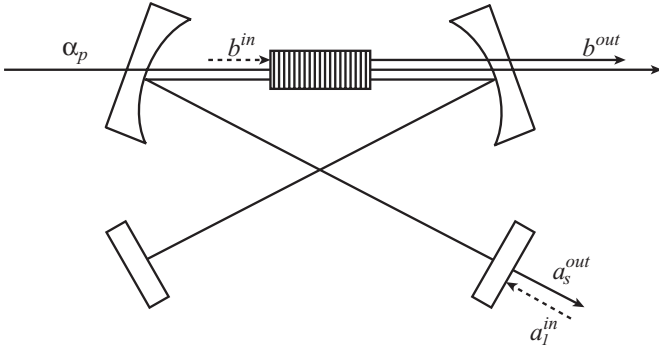


FIG. 1. The singly resonant OPO cavity scheme.  $\alpha_p$  is the input pump amplitude,  $a_s^{\text{in}}$  and  $b^{\text{in}}$  are the input signal and idler fields, and  $a_s^{\text{out}}$  and  $b^{\text{out}}$  are the output signal and idler fields.

of the field external to the cavity and coupled to the signal because of nonperfect reflection of the mirrors [16];  $H_{\text{int},1}$  in the Hamiltonian (3) represents the interaction of the signal mode with this heat bath, describing the damping of the signal mode caused by the nonzero transmittivity of the cavity;  $H_{\text{bath},2}$  is the free energy of different bosonic heat bath modes  $c_2(\omega)$  while the term  $H_{\text{int},2}$  is the interaction between the signal field and these modes, describing the damping of the signal mode associated with other loss mechanisms, like other mirror transmissions or crystal absorptions and diffraction; the term  $H_{\text{int},3}$  is the interaction between signal and idler modes and the pump field  $\alpha_p$  describing the process of parametric down-conversion inside the nonlinear crystal [6]. In the rotating-wave approximation, all these terms have explicit forms given by

$$H_{\text{sys}} = \hbar\omega_s a_s^\dagger a_s + \hbar \int_{-\infty}^{\infty} d\omega \omega b^\dagger(\omega) b(\omega), \quad (4)$$

$$H_{\text{bath},1} = \hbar \int_{-\infty}^{\infty} d\omega \omega c_1^\dagger(\omega) c_1(\omega), \quad (5)$$

$$H_{\text{bath},2} = \hbar \int_{-\infty}^{\infty} d\omega \omega c_2^\dagger(\omega) c_2(\omega), \quad (6)$$

$$H_{\text{int},1} = i\hbar \int_{-\infty}^{\infty} d\omega \kappa_1 [c_1(\omega) a_s^\dagger - c_1^\dagger(\omega) a_s], \quad (7)$$

$$H_{\text{int},2} = i\hbar \int_{-\infty}^{\infty} d\omega \kappa_2 [c_2(\omega) a_s^\dagger - c_2^\dagger(\omega) a_s], \quad (8)$$

$$H_{\text{int},3} = i\hbar \int_{-\infty}^{\infty} d\omega \kappa_3 [b^\dagger(\omega) a_s^\dagger \alpha_p - b(\omega) a_s \alpha_p^*]. \quad (9)$$

The coupling constants  $\kappa_1$ ,  $\kappa_2$ , and  $\kappa_3$  are considered to be independent of the frequency  $\omega$  according to the Markov approximation. We also consider the following commutation relations for the modes:

$$[a_s, a_s^\dagger] = 1, \quad (10)$$

$$[c_i(\omega), c_i^\dagger(\omega')] = \delta(\omega - \omega'), \quad (11)$$

$$[b(\omega), b^\dagger(\omega')] = \delta(\omega - \omega'), \quad (12)$$

where  $i = 1, 2$  while all the other commutators are identically zero. For the nonresonant idler field we use the theory of Collett and Levien [13], who showed that systems described by a continuum of mode operators  $\bar{b}(\omega)$  and possessing an

isolated mode of particular interest can be redescribed in terms of an orthonormal set formed by this one mode and a new continuum  $b(\omega)$ . From (3)–(9) one can derive a linearized Heisenberg-Langevin equation of motion for the fluctuations of the signal field below the threshold of oscillation in the interaction picture:

$$\frac{d}{dt} a_s = \gamma(\varepsilon^2 - 1) a_s - \sqrt{2\gamma\varepsilon} b^{\text{in}} + \sqrt{2\gamma_1} a_1^{\text{in}} + \sqrt{2\gamma_2} a_2^{\text{in}}, \quad (13)$$

where  $b^{\text{in}}$  is the idler field noise,  $\gamma_1 = \kappa_1^2 \pi$  is the signal cavity damping rate, and  $a_1^{\text{in}}$  are the input vacuum modes entering the cavity from the environment. The term  $\gamma_2 = \kappa_2^2 \pi$  is the intracavity loss rate, mainly due to absorption by the crystal, while  $a_2^{\text{in}}$  is the quantum noise associated with this loss and defined in the usual way [15]. We also consider  $\gamma = \gamma_1 + \gamma_2$  as the total damping rate and  $\varepsilon$  to parametrize the pump value below threshold  $\alpha_p = \varepsilon \alpha_{\text{th}}$ , where  $\alpha_{\text{th}} = \sqrt{\gamma/(\pi k_3^2)}$  so that  $0 < \varepsilon < 1$ . Note that there is no detuning in Eq. (13) since any change in the cavity length is compensated by a change in the signal (and idler) frequency, a property typical of SROPO configurations. In addition to the Langevin equation (13) there are boundary conditions, known as input-output relations:

$$a_s^{\text{out}} = \sqrt{2\gamma_1} a_s - a_1^{\text{in}}, \quad (14)$$

$$b^{\text{out}} = \varepsilon \sqrt{2\gamma} a_s^\dagger - b^{\text{in}}. \quad (15)$$

Note that the input-output relation of the signal field is written at the cavity mirror of the SROPO while that of the idler field makes explicit the propagation of the idler fluctuations through the crystal (see Fig. 1). The input fields satisfy the following commutation relations:

$$[a_i^{\text{in}}(t), a_i^{\text{in}}(t')] = \delta(t - t'), \quad (16)$$

$$[b^{\text{in}}(t), b^{\text{in}}(t')] = \delta(t - t'), \quad (17)$$

where  $i = 1, 2$ . Similar relations hold for the output fields while all the other commutators are vanishing.

For completeness we present the explicit expressions for the input and output fields, following the usual definition of [11]:

$$\begin{aligned} a_i^{\text{in}}(t) &= -\frac{1}{\sqrt{2\pi}} \int_{-\infty}^{+\infty} d\omega e^{-i\omega(t-t_0)} c_i^0(\omega), \\ b^{\text{in}}(t) &= -\frac{1}{\sqrt{2\pi}} \int_{-\infty}^{+\infty} d\omega e^{-i\omega(t-t_0)} b^0(\omega), \\ a_i^{\text{out}}(t) &= \frac{1}{\sqrt{2\pi}} \int_{-\infty}^{+\infty} d\omega e^{-i\omega(t-t_1)} c_i^1(\omega), \\ b^{\text{out}}(t) &= \frac{1}{\sqrt{2\pi}} \int_{-\infty}^{+\infty} d\omega e^{-i\omega(t-t_1)} b^1(\omega), \end{aligned} \quad (18)$$

where  $i = 1, 2$ ,  $t_0 < t$  and  $c_i^0(\omega)$  and  $b^0(\omega)$  are the values of  $c_i(\omega)$  and  $b(\omega)$  at  $t = t_0$ , respectively, while  $t_1 > t$  and  $c_i^1(\omega)$  and  $b^1(\omega)$  are the values of  $c_i(\omega)$  and  $b(\omega)$  at  $t = t_1$ , respectively. We consider the input noise to be a Gaussian-distributed white noise and the heat bath to be at zero temperature. In this basis the correlation functions for the input fields are

$$\langle a_i^{\text{in}}(t) a_i^{\text{in}}(t') \rangle = \langle b^{\text{in}}(t) b^{\text{in}}(t') \rangle = \delta(\tau), \quad (19)$$

where  $i = 1, 2$  and where we have defined  $\tau = t - t'$ .

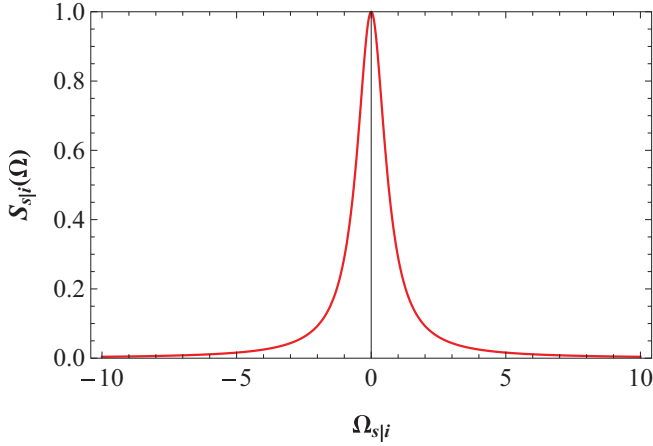


FIG. 2. (Color online) Signal or idler spectrum of Eq. (21) for  $\varepsilon = 0.8$ .

Quantities that can be readily calculated are the signal and idler output spectra. For the signal field, the spectrum is defined as

$$S_s(\omega) = \int_{-\infty}^{+\infty} d\tau \langle : a_s^{\dagger out}(0) a_s^{out}(\tau) : \rangle e^{i\omega\tau}, \quad (20)$$

where the symbols  $\langle : \cdot : \rangle$  denote time averaging and normal ordering, respectively, and with an analogous expression valid for the idler field. By using formal solutions of the Langevin equation (13), it is possible to evaluate the signal and idler spectra as functions of the normalized pump amplitude  $\varepsilon$ :

$$S_{s|i}(\Omega) = \frac{(1 - \varepsilon^2)^2}{(1 - \varepsilon^2)^2 + \Omega_{s|i}^2}, \quad (21)$$

where  $s|i$  means either signal or idler field, and we have defined  $\Omega_{s|i} = (\omega - \omega_{s|i})/\gamma$  and normalized to the value of the spectrum at resonance. The spectrum of Eq. (21) is shown in Fig. 2; the spectra for signal and idler fields are two Lorentzians centered at the signal and idler frequencies, respectively. Although the idler is not resonant, this field still experiences the presence of the cavity because of the frequency entanglement which is peculiar to the process of parametric down-conversion in the crystal.

### III. DIRECT DETECTION OF INTENSITY FLUCTUATIONS

Direct detection of intensity fluctuations of signal and idler fields is the simplest type of measurement one can perform in a two-color OPO. A reduction in the intensity difference fluctuations below the shot-noise level in doubly resonant OPOs above the threshold of oscillation was calculated by Reynaud *et al.* [17] and Lane *et al.* [18] and demonstrated by Heidmann *et al.* [19] for a type-II nondegenerate OPO. Here we extend these approaches to include the study of signal-idler intensity fluctuations in a SROPO below the threshold of oscillation. In this type of measurement the signal and idler fields hit two different photodetectors and then the resulting intensity-difference fluctuations are studied with a power spectrum analyzer. The measurable output is related to

the Fourier transform of the intensity-difference correlation function:

$$\frac{S_D[\omega]}{S_0} = 1 + \frac{1}{S_0} \int_{-\infty}^{+\infty} d\tau \langle : I_D^{out}(0), I_D^{out}(\tau) : \rangle e^{i\omega\tau}, \quad (22)$$

where  $I_D^{out}(t) = a_s^{\dagger out}(t)a_s^{out}(t) - b^{\dagger out}(t)b^{out}(t)$  is the output intensity-difference operator for signal and idler fields,  $S_0$  is the shot-noise level given in this case by the sum of the intensities of signal and idler beams,  $S_0 = I_s^{out} + I_l^{out}$ . Furthermore, for any operators  $A$  and  $B$ :

$$\langle A, B \rangle = \langle AB \rangle - \langle A \rangle \langle B \rangle. \quad (23)$$

From the solution of Eq. (13) one can calculate the squeezing spectrum of the intensity-difference correlation analytically:

$$\frac{S_D[\Omega]}{S_0} = 1 - \frac{8(\Gamma - \varepsilon^2)(1 - \Gamma\varepsilon^2)}{(1 + \Gamma)[4(1 - \varepsilon^2)^2 + \Omega^2]}, \quad (24)$$

where we have defined  $\Gamma = \gamma_1/\gamma$ . The spectrum (24) is shown in Fig. 3(a) for different values of the pump parameter  $\varepsilon$  and for  $\Gamma = 1$  (i.e.  $\gamma_2 = 0$ ). In this case (24) reduces to:

$$\frac{S_D[\Omega]}{S_0} = 1 - \frac{4}{4 + [\Omega/(1 - \varepsilon^2)]^2}, \quad (25)$$

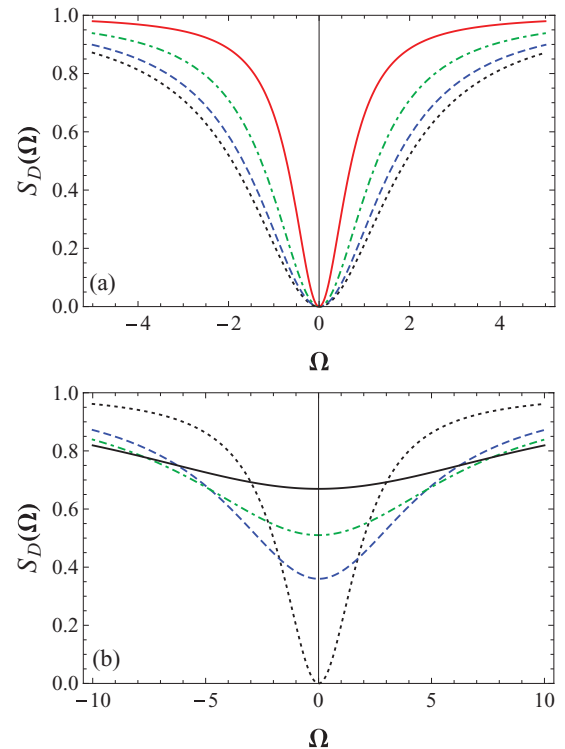


FIG. 3. (Color online) (a) Intensity-difference correlation spectrum of (25) plotted for a range of input powers and  $\Gamma = 1$ . Curves correspond to  $\varepsilon = 0.2$  (black dotted line),  $\varepsilon = 0.4$  (blue dashed line),  $\varepsilon = 0.6$  (green dash-dotted line), and  $\varepsilon = 0.8$  (red solid line). (b) Intensity-difference correlation spectrum of (26) plotted for a range of  $Z = \gamma_i/\gamma_s$  values. Curves correspond to  $Z = 1$  (black dotted line),  $Z = 4$  (blue dashed line),  $Z = 6$  (green dash-dotted line), and  $Z = 10$  (black solid line).

where a narrowing of the spectrum when approaching threshold clearly confirms the plots of Fig. 3. The dependence of the spectrum (24),(25) on the pump parameter, which leads to the progressive narrowing of the spectral line when threshold is approached, is peculiar to the singly resonant case. No dependence on the pump is in fact observed in the doubly resonant OPO where the spectrum has the following analytical expression [7,20]:

$$\frac{S_D[\Omega]}{S_0} = 1 - \frac{4}{\frac{\Omega^2}{\gamma_s \gamma_i} + \left[ \sqrt{\frac{\gamma_s}{\gamma_i}} + \sqrt{\frac{\gamma_i}{\gamma_s}} \right]^2}, \quad (26)$$

where  $\gamma_s$  and  $\gamma_i$  are the signal and idler cavity decay rates. In order to study the behavior of the SROPO configuration, one may be tempted to use Eq. (26) in the limit of  $\gamma_s$  or  $\gamma_i$  approaching infinity. In this case Eq. (26) would reach the asymptotic value of 1 [see Fig. 3(b) where  $Z = \gamma_i/\gamma_s$  is increased from 1 to 10], meaning that no squeezing would be observable in such a measurement. Such a limit, however, is not well posed mathematically since it breaks the mean-field-limit approximation used in the derivation of Eq. (26). Our calculations predict instead that the narrowing of the spectral line is a function of the pump parameter  $\varepsilon$  and that squeezing below the shot noise is indeed possible in the SROPO. It is worth noting that, analogously to the doubly resonant case, perfect suppression of noise below the shot noise level is achievable at resonance, independently of the pump power in SROPO.

#### IV. PHASE-SENSITIVE MEASUREMENTS

The intensity correlation function calculated in Sec. III contains no phase information since it is a measure of the fluctuations in the photon numbers. A useful approach to characterize squeezing is a phase-sensitive scheme that measures the variance of field quadratures, as shown in [21,22]. Such a scheme is based on homodyne detection and consists of superposing the input field on the field from a strong local oscillator. In this section we consider the case in which the signal and idler beams from the SROPO are spatially separated and then combined separately with their own local oscillators, one at the frequency of the signal and the other at the frequency of the idler field, before hitting two different photodetectors. The fluctuations in the signal-idler intensity difference are then investigated with the use of a power spectrum analyzer. In this case the measurable output is related to the Fourier transform of signal-idler quadrature difference fluctuations:

$$V_D[\omega] = 1 + \int_{-\infty}^{+\infty} d\tau \langle : X_D(0) X_D(\tau) : \rangle e^{i\omega\tau}, \quad (27)$$

where  $X_D(t) = X_\theta^s(t) - X_\phi^i(t)$  and

$$\begin{aligned} X_\theta^s(t) &= a_s(t)e^{i(\theta+\omega_s t)} + a_s^\dagger(t)e^{-i(\theta+\omega_s t)}, \\ X_\phi^i(t) &= b(t)e^{i(\phi+\omega_i t)} + b^\dagger(t)e^{-i(\phi+\omega_i t)} \end{aligned} \quad (28)$$

are the quadrature operators for signal and idler beams corresponding to the angles  $\theta$  and  $\phi$ , respectively.

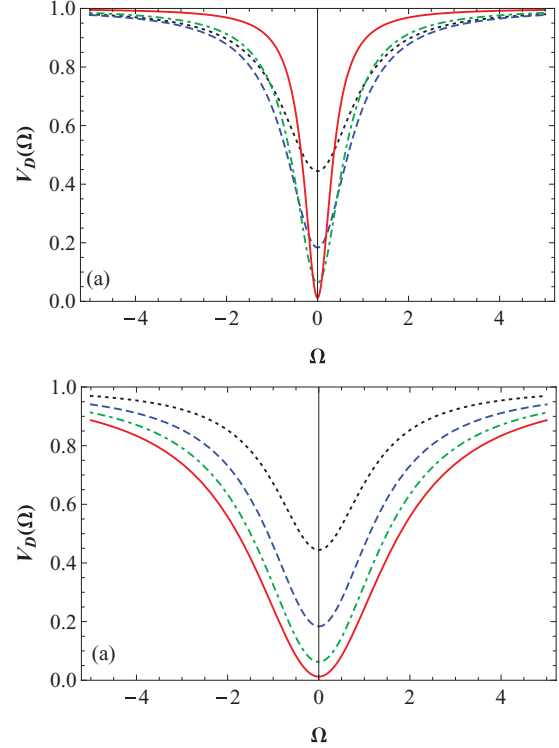


FIG. 4. (Color online) (a) Quadrature squeezing spectrum (29) for a range of input powers and  $\Gamma = 1$ . Curves correspond to  $\varepsilon = 0.2$  (black dotted line),  $\varepsilon = 0.4$  (blue dashed line),  $\varepsilon = 0.6$  (green dash-dotted line), and  $\varepsilon = 0.8$  (red solid line). (b) Quadrature squeezing spectrum in the doubly resonant case for a range of input powers and  $Z = \gamma_i/\gamma_s = 1$ . Curves correspond to  $\varepsilon = 0.2$  (black dotted line),  $\varepsilon = 0.4$  (blue dashed line),  $\varepsilon = 0.6$  (green dash-dotted line), and  $\varepsilon = 0.8$  (red solid line). Only minimal fluctuations corresponding to  $\theta + \phi = 0$  are shown.

Lengthy calculations provide the quadrature squeezing spectrum:

$$V_D[\Omega] = 1 + \frac{4\varepsilon[(1+\Gamma)\varepsilon - \sqrt{\Gamma}(1+\varepsilon^2)\cos(\theta+\phi)]}{(1-\varepsilon^2)^2 + \Omega^2}. \quad (29)$$

The spectrum (29) is shown in Fig. 4(a) for different values of the pump parameter  $\varepsilon$  and for  $\Gamma = 1$ . In this case Eq. (29) reduces to

$$V_D[\Omega] = 1 - \frac{4\varepsilon}{(1+\varepsilon)^2 + [\Omega/(1-\varepsilon)]^2}, \quad (30)$$

showing again a line narrowing when threshold is approached. This result should be contrasted with that for the doubly resonant OPO, where one obtains the same formula (30) for  $Z = \gamma_i/\gamma_s = 1$  after replacing  $\Omega/(1-\varepsilon) = \Delta$  and where no line narrowing is observed [8,22]. This is made clear in the plots of Fig. 4(b). The singly and doubly resonant cases, however, have coincident spectra at  $\Omega = 0$ . The squeezing spectrum is symmetric around  $\Omega = 0$ , which corresponds to the local oscillator frequencies  $\omega_{s|i}$ . One important difference with the intensity case of Sec. III is that a progressive growth in the squeezing level is observed when the threshold of oscillation is approached.

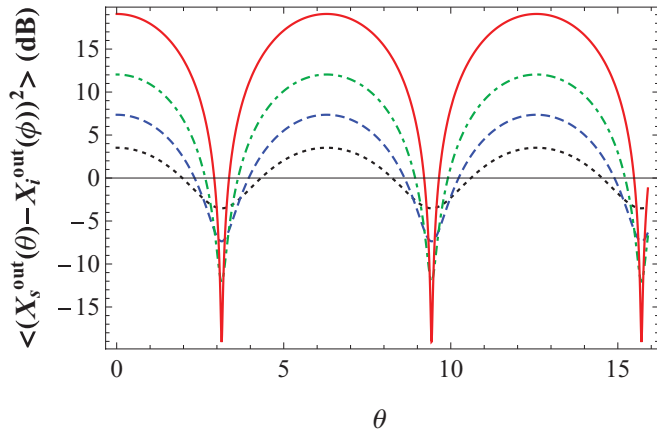


FIG. 5. (Color online) Quantum fluctuations of the signal-idler quadrature difference at  $\omega = \omega_{s|i}$  for several values of the pump parameter  $\varepsilon$  and  $\Gamma = 1$ .  $\phi$  is kept constant while  $\theta$  is scanned linearly. Curves correspond to  $\varepsilon = 0.2$  (black dotted line),  $\varepsilon = 0.4$  (blue dashed line),  $\varepsilon = 0.6$  (green dash-dotted line), and  $\varepsilon = 0.8$  (red solid line).

Another useful way to visualize squeezing is shown in Fig. 5 where we plot the quantum fluctuations of the signal-idler quadrature difference at  $\omega = \omega_{s|i}$  in a decibel scale with respect to the shot-noise level obtained by blocking the SROPO pump. The plot is obtained by keeping the phase  $\phi$  of one of the two local oscillators fixed while varying the phase  $\theta$  of the other. The shot-noise level or standard quantum limit is represented by the zero black line. It is evident that a large amount of squeezing ( $-19$  dB) can, in principle, be obtained in this situation.

Figure 6 displays the noise spectrum as a function of the normalized pump amplitude in the case in which the signal field experiences other losses besides those due to the mirror transmittance ( $\Gamma = 0.8$  in this plot). Figure 7 shows the signal-idler quadrature fluctuations for  $\Gamma = 0.8$  for several values of the pump parameter as a function of  $\theta$ , the phase of the signal local oscillator. It is clear from these figures that the squeezing level is severely affected by other asymmetric loss mechanisms and that squeezing degradation becomes more important as we approach threshold. The degradation of squeezing in Figs. 6 and 7 reflects the difficulty in achieving noise cancellation

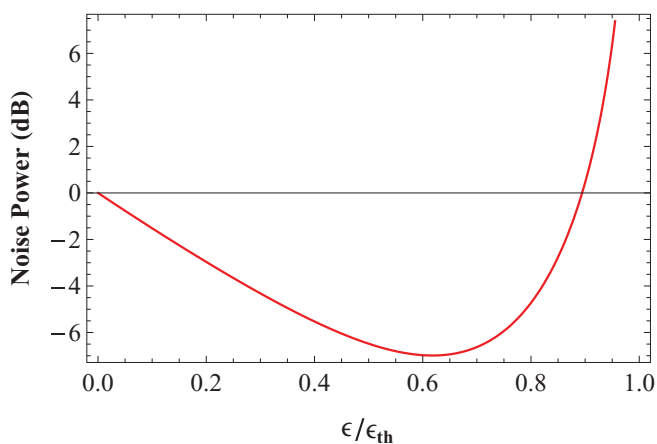


FIG. 6. (Color online) Noise power at resonance as a function of normalized pump amplitude. Here  $\varepsilon = 0.6$  and  $\Gamma = 0.8$ .

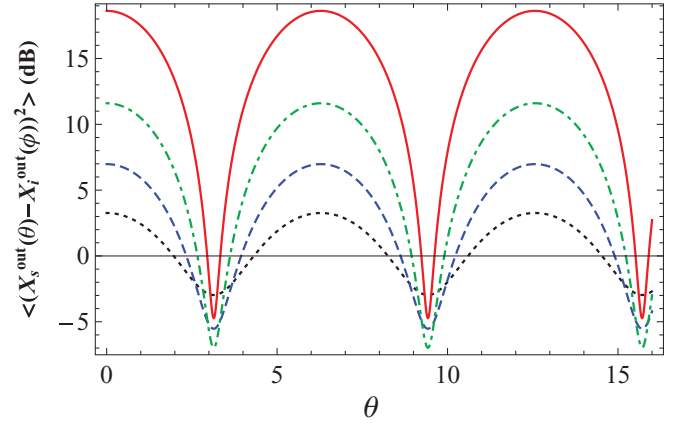


FIG. 7. (Color online) Quantum fluctuations of the signal-idler quadrature difference at  $\omega = \omega_{s|i}$  for several values of the pump parameter  $\varepsilon$  and  $\Gamma = 0.8$ . Curves correspond to  $\varepsilon = 0.2$  (black dotted line),  $\varepsilon = 0.4$  (blue dashed line),  $\varepsilon = 0.6$  (green dash-dotted line), and  $\varepsilon = 0.8$  (red solid line).  $\phi$  is kept constant while  $\theta$  is scanned linearly in time.

in the signal-idler intensity for an asymmetric cavity in the presence of growth of the single beam noise. It is, however, possible to compensate for this behavior by introducing the optimal squeezing angle [8]. In the case where signal and idler beams experience other asymmetric losses, the symmetric combination of quadrature operators in Eq. (27) is no longer the best choice and we have to use a more general linear combination of signal-idler quadrature operators parametrized by an angle  $\psi$ :

$$X_D(t) = \cos(\psi)X_\theta^s(t) - \sin(\psi)X_\phi^i(t). \quad (31)$$

In this more general case the calculated squeezing spectrum turns out to be

$$V_D[\Omega] = 1 + \frac{4\varepsilon\{2\varepsilon\cos^2[\psi] + 2\Gamma\varepsilon\sin^2[\psi] - \sqrt{\Gamma}(1 + \varepsilon^2)\sin[2\psi]\}}{(-1 + \varepsilon^2)^2 + \Omega^2}. \quad (32)$$

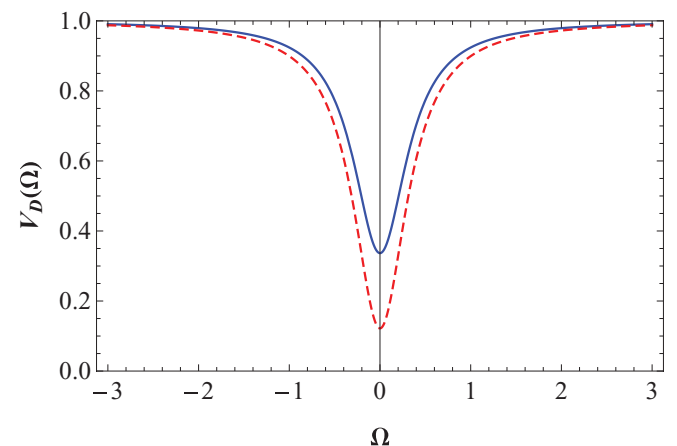


FIG. 8. (Color online) Optimized quadrature spectrum. In this case  $\Gamma = 0.8$ ,  $\varepsilon = 0.8$ , and  $\psi = \pi/4$  (blue solid line),  $\psi = \psi_0$  (red dashed line).

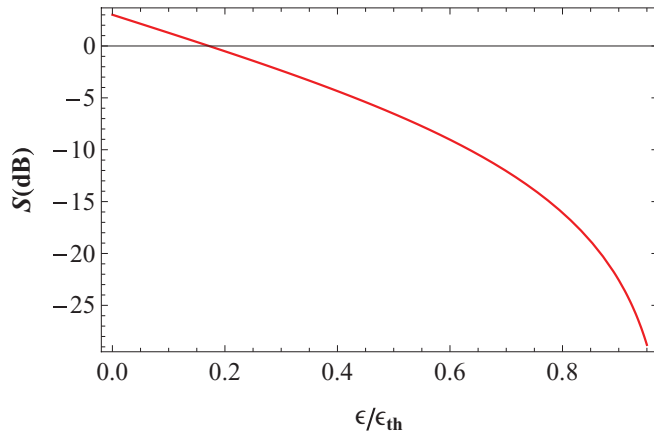


FIG. 9. (Color online) Amount of entanglement as a function of the normalized pump value. The decibel scale is evaluated with respect to the value 2 which sets the limit of state separability in Eq. (34).  $\Gamma = 1$  in this figure.

The optimization of signal-idler correlations is achieved by minimizing Eq. (32) with respect to  $\psi$  for a given fixed value of all the other parameters and by choosing the frequency  $\Omega$  where minimal fluctuations occur (in our case  $\Omega = 0$ ). The optimal angle  $\psi_0$  is found from the implicit equation

$$\tan(2\psi_0) = \frac{\sqrt{\Gamma}(1 + \varepsilon^2)}{(1 - \Gamma)\varepsilon}. \quad (33)$$

The squeezing spectrum plotted in Fig. 8 for  $\Gamma = 0.8$  and  $\varepsilon = 0.8$  shows a nonoptimal choice of the angle  $\psi$  (narrower curve) and an optimal one (broader curve). From this figure it is evident that by operating at the optimal choice of the angle  $\psi$  one obtains an improvement in the squeezing level.

## V. QUANTUM ENTANGLEMENT

In order to claim state inseparability and consequently entanglement for the signal-idler state we apply the separability criterion of Simon [23] and Duan *et al.* [24]. According to this criterion a sufficient condition for state inseparability is that the quantity

$$S = \left( \langle [X_\theta^s - X_\phi^i]^2 \rangle + \langle [X_{\theta+\pi/2}^s + X_{\phi+\pi/2}^i]^2 \rangle \right) \quad (34)$$

is such that

$$S < 2. \quad (35)$$

We have calculated  $S = 0.024$  for the case where  $\varepsilon = 0.8$  and  $\Gamma = 1$ ;  $S = 0.67$  for  $\varepsilon = 0.8$ ,  $\Gamma = 0.8$ , and  $\psi = \pi/4$ ; and finally,  $S = 0.5$  for  $\Gamma = 0.8$ ,  $\varepsilon = 0.8$ , and  $\psi = \psi_0$ . Hence we conclude that the signal and idler beams are in an entangled state for wide ranges of parameter values and different configurations of operation on a SROPO. The dependence of the amount of entanglement on the normalized pump value is shown in Fig. 9 where the decibel scale is evaluated with respect to the value 2 which sets the limit of state separability in Eq. (34).

## VI. CONCLUSIONS

We have applied the input-output theory of [16] to study the quantum fluctuations of singly resonant optical parametric oscillators. The model has been used to calculate intensity and quadrature squeezing spectra. We have shown that below the threshold of oscillation the fluctuations in the light outside the cavity at the frequencies of the signal and the idler fields are squeezed below the shot noise as much as in the doubly resonant case. We have also shown that signal and idler fields are entangled over a wide range of pump parameter values in the SROPO by using the Simon–Duan *et al.* criterion of state separability.

One major difference of the SROPO from the doubly resonant case is that we observe an unexpected dependence of the intensity-difference spectrum on the pump parameter, leading to a narrowing of the spectral line as the threshold of oscillation is approached. An analogous dependence of the quadrature spectrum on the pump parameter is also found. A peculiar feature of singly resonant configurations is that the narrowing of the spectral lines does not affect the squeezing minimum, which can reach values similar to those of the doubly resonant case as threshold is approached. Since the singly resonant cavity is one of the simplest OPO configurations to realize, and since there is no difference in the squeezing properties of the light coming from this device with respect to the doubly resonant cavity, we conclude that the singly resonant configuration could be an ideal candidate for the realization of two-color entangled light in quantum information processes.

## ACKNOWLEDGMENTS

We thank J. Jeffers, F. Papoff, and C. Fabre for useful discussions. We acknowledge financial support from the EU commission through the IST network project HIDEAS (Grant No. FP7-ICT-221906).

- [1] P. Grangier, R. E. Slusher, B. Yurke and A. La Porta, *Phys. Rev. Lett.* **59**, 2153 (1987).
- [2] M. Xiao, L. A. Wu, and H. J. Kimble, *Phys. Rev. Lett.* **59**, 278 (1987).
- [3] C. M. Caves, *Phys. Rev. Lett.* **45**, 75 (1980).
- [4] A. F. Pace, M. J. Collett, and D. F. Walls, *Phys. Rev. A* **47**, 3173 (1993).
- [5] S. L. Braunstein and P. Van Loock, *Rev. Mod. Phys.* **77**, 513 (2005).

- [6] L. Mandel and E. Wolf, *Optical Coherence and Quantum Optics* (Cambridge University Press, Cambridge, 1995).
- [7] C. Fabre, E. Giacobino, A. Heidmann, and S. Reynaud, *J. Phys. (France)* **50**, 1209 (1989).
- [8] C. Schori, J. L. Sorensen, and E. S. Polzik, *Phys. Rev. A* **66**, 033802 (2002).
- [9] J. Laurat, T. Coudreau, G. Keller, N. Treps, and C. Fabre, *Phys. Rev. A* **71**, 022313 (2005).

- [10] C. W. Gardiner and P. Zoller, *Quantum Noise* (Springer, Berlin, 2004).
- [11] D. F. Walls and Gerard J. Milburn, *Quantum Optics* (Springer, Berlin, 2008).
- [12] I. N. Agafonov, M. V. Chekhova, and G. Leuchs, *Phys. Rev. A* **82**, 011801(R) (2010).
- [13] M. J. Collett and R. B. Levien, *Phys. Rev. A* **43**, 5068 (1991).
- [14] R. Paschotta, M. Collett, P. Kürz, K. Fiedler, H. A. Bachor, and J. Mlynek, *Phys. Rev. Lett.* **72**, 3807 (1994).
- [15] K. J. Blow, R. Loudon, S. J. D. Phoenix, and T. J. Shepherd, *Phys. Rev. A* **42**, 4102 (1990).
- [16] M. J. Collett and C. W. Gardiner, *Phys. Rev. A* **30**, 1386 (1984).
- [17] S. Reynaud, C. Fabre, and E. Giacobino, *J. Opt. Soc. Am. B* **4**, 1520 (1988).
- [18] A. S. Lane, M. D. Reid, and D. F. Walls, *Phys. Rev. A* **38**, 788 (1988).
- [19] A. Heidmann, R. J. Horowicz, S. Reynaud, E. Giacobino, C. Fabre, and G. Camy, *Phys. Rev. Lett.* **59**, 2555 (1987).
- [20] A. S. Lane, M. D. Reid, and D. F. Walls, *Phys. Lett.* **60**, 1940 (1988).
- [21] M. O. Scully and M. S. Zubairy, *Quantum Optics* (Cambridge University Press, Cambridge, 2008).
- [22] P. D. Drummond and M. D. Reid, *Phys. Rev. A* **41**, 3930 (1990).
- [23] R. Simon, *Phys. Rev. Lett.* **84**, 2726 (2000).
- [24] L. M. Duan, G. Giedke, J. I. Cirac, and P. Zoller, *Phys. Rev. Lett.* **84**, 2722 (2000).